Secondary Structure and Secondary Structure Dynamics of DNA Hairpins Complexed with HIV-1 NC Protein

Gonzalo Cosa,* Elizabeth J. Harbron,* Yining Zeng,* Hsiao-Wei Liu,* Donald B. O'Connor,* Chie Eta-Hosokawa,† Karin Musier-Forsyth,‡ and Paul F. Barbara*

*Department of Chemistry and Biochemistry, Center for Nano and Molecular Science and Technology, University of Texas, Austin, Texas 78712; †Department of Applied Physics, Osaka University, Suita, Osaka 565 0871, Japan; and ‡Department of Chemistry, University of Minnesota, Minneapolis, Minnesota 55455

ABSTRACT Reverse transcription of the HIV-1 RNA genome involves several complex nucleic acid rearrangement steps that are catalyzed by the HIV-1 nucleocapsid protein (NC), including for example, the annealing of the transactivation response (TAR) region of the viral RNA to the complementary region (TAR DNA) in minus-strand strong-stop DNA. We report herein single-molecule fluorescence resonance energy transfer measurements on single immobilized TAR DNA hairpins and hairpin mutants complexed with NC (i.e., TAR DNA/NC). Using this approach we have explored the conformational distribution and dynamics of the hairpins in the presence and absence of NC protein. The data demonstrate that NC shifts the equilibrium secondary structure of TAR DNA hairpins from a fully ''closed'' conformation to essentially one specific ''partially open'' conformation. In this specific conformation, the two terminal stems are ''open'' or unwound and the other stems are closed. This partially open conformation is arguably a key TAR DNA intermediate in the NC-induced annealing mechanism of TAR DNA.

INTRODUCTION

The HIV-1 nucleocapsid protein (NC) is a 55-amino-acid zinc-binding (Henderson et al., 1992; South et al., 1990; Summers et al., 1992) nucleic acid chaperone protein, which facilitates reverse transcription of the HIV-1 RNA genome by catalyzing the rearrangement of nucleic acid structures (Darlix et al., 1995; Herchslag 1995; Lorsch 2002; Rein et al., 1998; Tsuchihashi and Brown 1994). To achieve such rearrangements, certain basepair interactions must be broken, while other complementary basepair interactions must be formed, resulting in a thermodynamically more stable conformation.

Various steps in reverse transcription are catalyzed by NC. One such step is minus-strand strong-stop DNA ((−) SSDNA) strand transfer to the 3′ end of the RNA genome. This reaction is mediated by basepairing of the complementary repeat regions in (−) SSDNA and viral RNA. This process involves annealing of the transactivation response (TAR) RNA present in the viral RNA, to the complementary DNA sequence (TAR DNA) in (−) SSDNA. Both TAR RNA and TAR DNA sequences are predicted to fold into stable hairpin structures (Coffin et al., 1997; Guo et al., 1997; Kim et al., 1997; You and McHenry, 1994). These hairpin structures prevent the intermolecular annealing reaction resulting in the formation of a 98-nucleotide (nt) basepaired binary complex. NC has been shown to stimulate minus-strand transfer by increasing the rate of intermolecular annealing and by blocking a competing intramolecular self-priming reaction (Driscoll and Hughes, 2000; Guo et al., 1997; Lapadat-Tapolsky et al., 1997; You and McHenry, 1994), which occurs due to the presence of the TAR DNA hairpin at the 3′ end of the (−) SSDNA (Coffin et al., 1997; Guo et al., 1997; Kim et al., 1997; You and McHenry, 1994).

The effect of NC binding on the conformations of TAR DNA hairpins has previously been investigated by ensemble fluorescence resonance energy transfer (FRET) measurements and other techniques (Azoulay et al., 2003; Beltz et al., 2003; Bernacchi et al., 2002; Hong et al., 2003). These data demonstrate that bound NC shifts the TAR DNA hairpin equilibrium toward ''open'' conformations. However, the averaging inherent in ensemble FRET measurements makes it difficult to identify specific conformations (Azoulay et al., 2003; Beltz et al., 2003; Bernacchi et al., 2002; Hong et al., 2003). To obtain more detailed information on the conformations of TAR DNA/NC we undertook the first time-resolved single molecule fluorescence resonance energy transfer (SM-FRET) measurements on TAR DNA hairpins and hairpin mutants in the presence and absence of NC protein. Our single molecule results clearly demonstrate that bound NC shifts the equilibrium secondary structure of TAR DNA hairpins from a fully ''closed'' conformation to a specific ''partially open'' conformation with the two terminal stems ''open'' or unwound and the other stems closed. In addition, the data show that the two terminal stems in the TAR DNA/NC complex undergo a rapid opening/closing process. The observed partially open TAR DNA/NC conformation seems ideally suited for the promotion of NC catalyzed DNA/RNA annealing, because the open terminal stems possess 21 unpaired bases accessible for DNA/RNA annealing.

Submitted March 18, 2004, and accepted for publication June 17, 2004.

Address reprint requests to Paul F. Barbara, E-mail: p.barbara@mail.utexas.edu.

Elizabeth J. Harbron's present address is Dept. of Chemistry, The College of William and Mary, Williamsburg, VA 23187.

0006-3495/04/10/2759/09 $2.00

doi: 10.1529/biophysj.104.043083

MATERIALS AND METHODS

Protein and nucleic acids

HIV-1 NC was prepared as previously described (Lee et al., 1998). The dye-labeled DNA hairpins (64 mer, 67 mer, 68 mer, 70 mer, and 71 mer) were purchased from TriLink Biotechnologies (San Diego, CA), and their predicted secondary structures are shown in Fig. 1. Cy3 and Cy5 were chosen as the FRET donor and acceptor dyes, respectively. Cy3-amidite was directly coupled to the 5′ end of the DNA. Cy5-succinimidyl ester was postsynthetically coupled to an amino linker at the 3′ end of the DNA. To prevent the undesirable G residue quenching effects (Kurata et al., 2001; Torimura et al., 2001), a 5′-T and 3′-TTTT overhang were added to the core 59-mer TAR DNA sequence. The 3′ overhang also prevents formation of a dark nonfluorescent state that can form due to close proximity of the two dyes (see also Fig. S1 and the accompanying discussion in the Supplementary Material) (Bernacchi et al., 2002). To study fluorescence intensity time trajectories over long time periods, DNA hairpins were immobilized using the biotin-streptavidin interaction (Grunwell et al., 2001; Ha et al., 1999; Zhuang et al., 2000). A biotin was internally attached via a dT-biotin phosphoramidite reagent. The oligonucleotides were purified by the supplier by polyacrylamide gel electrophoresis and reversed-phase HPLC. Before hairpin immobilization on the coverslips (see below), the oligonucleotide solution was diluted to a final concentration of 25–50 pM in HEPES buffer (25 mM HEPES, pH 7.3, 40 mM NaCl) containing 10 mM $MgCl_2$ and reannealed by incubation for 2.5 min at 80°C, 2.5 min at 60°C, and 5 min at 0°C.

Hairpin immobilization

Predrilled polycarbonate films with an adhesive gasket (Grace Bio-Labs, Bend, OR) were assembled on top of cleaned coverslips yielding a chamber with a total volume of ~10 μL. Inlet and outlet ports (Nanoport, Upchurch Scientific, Oak Harbor, WA) were glued on top of the chambers. The chambers were incubated sequentially for 10 min with solutions of biotinylated bovine serum albumin (BSA) (Pierce Biotechnology, Rockport, IL; 2 mg/mL in distilled deionized water) and streptavidin (Molecular Probes, Eugene, OR; 0.2 mg/mL in HEPES buffer). The chambers were rinsed with distilled deionized water (50 μL) after each incubation step. The doubly labeled oligomer solution (25–50 pM) was incubated subsequently for 20 min. The chambers were rinsed and Teflon tubing was adapted to the chamber ports. Two syringe pumps delivered solutions at a rate of 2 μl/min. A 5-min equilibration period at a flow rate of 10 μl/min was elapsed before measurements were taken under a new set of conditions (e.g., addition of NC). All solutions consisted of HEPES buffer containing 0.2 mM $MgCl_2$ and an oxygen scavenger system (2-mercaptoethanol 1% v/v (Sigma-Aldrich, St. Louis, MO), β-D(+)glucose 3% w/v (Sigma-Aldrich), glucose oxidase 0.1 mg/mL (Roche Applied Science, Hague Road, IN), and catalase 0.02 mg/mL (Roche Applied Science)) (Ha, 2001; Harada et al., 1990).

Single molecule spectroscopy on the dye-labeled hairpins with polarized excitation and modulation of the direction of polarized light demonstrated that the dyes were freely rotating (data not shown). This is consistent with successful immobilization of the hairpins without undesirable interactions of the hairpin-dye structures with the surface of the coverslip.

Experimental setup

The experimental setup has been described previously (English et al., 2000; Yip et al., 1998). A closed-loop sample scanning stage (NPS-XY-100A, Queensgate, Torquay, Devon, UK) was used for imaging and sample positioning. Continuous wave excitation (514 nm, ~5–10 μW/μm^2) from an argon ion laser (model Reliant 150m, Laser Physics, West Jordan, UT) was introduced via an optical fiber and was directed by a dichroic beamsplitter (530 DCLP, Chroma, Rockingham, VT) to the sample via a high numerical aperture (N.A.) oil immersion microscope objective (Zeiss Fluar, 100×, N.A. 1.3) (Carl Zeiss, Oberkochen, Germany). Fluorescence from the sample passed through the dichroic beamsplitter and a holographic Raman notch filter (Kaiser Optical Systems, Ann Arbor, MI) and was then directed to the detectors by means of an internal mirror. Imaging of the sample and measurement of single molecule fluorescence intensity time trajectories were conducted using two avalanche photodiode (APD) detectors (Perkin Elmer Optoelectronics SPCM-AQR-15, Vaudreuil, Quebec, Canada). The collected fluorescence was separated into donor and acceptor channels by a dichroic beam splitter (Chroma 630 DCXR). The TTL output signal from the APDs was distributed by a 1:4 fanout TTL driver (Pulse Research Lab, Torrance, CA) into an ALV 5000/E (ALV-Laser, Langen, Hessen, Germany) correlation board and a counter board. This configuration allowed us to simultaneously obtain intensity time trajectories with 1-ms time resolution and donor-acceptor intensity cross correlation with 0.5-μs time resolution for each single molecule.

Data analysis

Single hairpin fluorescence intensity time trajectories were recorded using separate donor and acceptor channels, each with an APD detector. The signals $S_i(t)$ were corrected for background emission and donor/acceptor cross talk due to overlapping emission using Eq. 1:

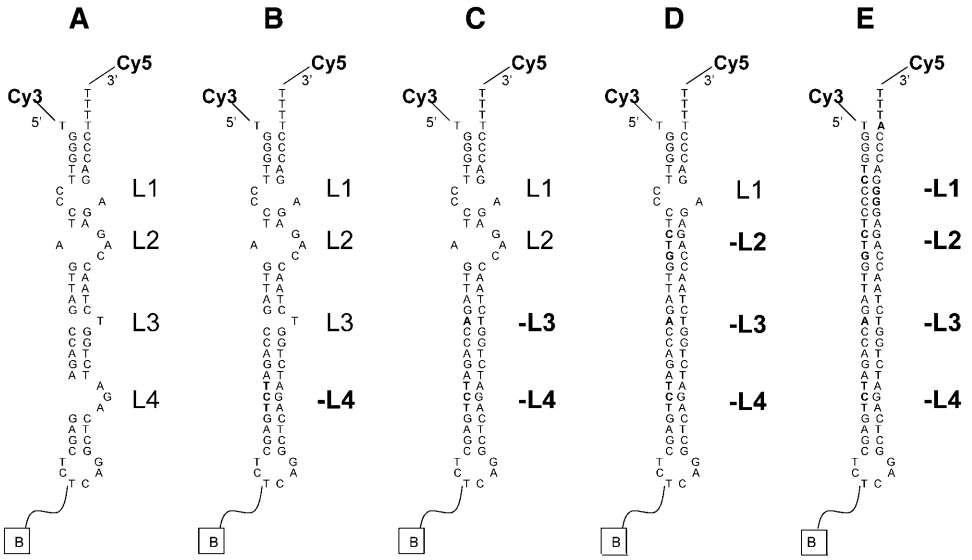

FIGURE 1 Structures of the oligonucleotides employed in the single molecule FRET studies. (*A*) Predicted secondary structure of the TAR DNA hairpin (64-nt); Cy3 was used as the donor dye molecule and was coupled to the 5′-dT of the DNA. Cy5 was used as the acceptor dye molecule and was attached to the 3′-dT of the DNA. (*B*) A 67-nt TAR DNA mutant for which one internal bulge was deleted (-L4). (*C*) A 68-nt TAR DNA mutant for which two internal bulges were deleted (-L4-L3). (*D*) A 70-nt TAR DNA mutant for which three internal bulges were deleted (-L4-L3-L2). (*E*) A 71-nt TAR DNA mutant for which the four internal bulges were deleted (-L4-L3-L2-L1). The DNAs were attached to the surface via a biotin linker (*B*) attached to a dT in the hairpin loop region.

$$I_i(t) = S_i(t) - B_i(t) - C_i \quad (1)$$

where i is donor or acceptor, $I_i(t)$ is the corrected fluorescence intensity of the donor/acceptor dye, $B_i(t)$ is the background, and C_i the cross talk between the donor and acceptor channels (Ying et al., 2000). The simultaneous detection of both donor $I_D(t)$ and acceptor $I_A(t)$ fluorescence intensity time trajectories can be used to calculate the time trajectory of the FRET efficiency, $E_{FRET}(t)$, as shown in Eq. 2, where Φ_A and Φ_D are the emission quantum yields of acceptor and donor dyes, respectively, and η_A and η_D are the acceptor and donor detector efficiencies, respectively. Single molecule $E_{FRET}(t)$ trajectories reflect the time trajectory of the end-to-end distance $R(t)$ in the donor-acceptor pair as observed in Eq. 3 (Lakowicz, 1999):

$$E_{FRET}(t) = \frac{I_A(t)}{I_A(t) + I_D(t) \times \dfrac{(\phi_A \times \eta_A)}{(\phi_D \times \eta_D)}} \quad (2)$$

$$E_{FRET}(t) = \frac{R_o^6}{R_o^6 + R(t)^6} \quad (3)$$

where R_o is the Förster radius, the distance at which energy transfer is 50% efficient. We have used an $R_o = 60$ Å, measured for Cy3-Cy5 when coupled to DNA (Ha et al., 2002).

The correction factor for emission and detection efficiencies ($\Phi_A \times \eta_A$ / $\Phi_D \times \eta_D$) is ~1 under our experimental conditions, thus the apparent FRET efficiency $E_{app}(t)$, given by the ratio of acceptor to the sum of acceptor plus donor intensities is equal to $E_{FRET}(t)$. The correction factor was determined by comparing the emission from acceptor dye under 100% energy transfer efficiency and the emission from the donor-only subpopulation of molecules.

Blinking events (acceptor reversible photobleaching) were removed before data analysis. A threshold criterion was applied to the counts on the acceptor channel. This criterion removes experimental points where the acceptor intensity is due to background and/or cross talk from the donor channel. The threshold criterion equals 2× the combined uncertainty on the acceptor channel (S_A) resulting from the background (SB_A) and the cross talk (SC_A), as shown in Eq. 4.

$$2 \times S_A = 2 \times \sqrt{SB_A^2 + SC_A^2} \quad (4)$$

Assuming that the only source of uncertainties is photon shot noise in the background and the cross talk, Eq. 4 rearranges to:

$$2 \times S_A = 2 \times \sqrt{\langle B_A \rangle + \langle C_A \rangle}$$

where $\langle B_A \rangle$ is the average background intensity in the acceptor channel and $\langle C_A \rangle$ is the average cross talk from donor into acceptor channel before acceptor photobleaching. (Note that for simplicity we have approximated C_A as a constant value; C_A is, however, dependent on the donor intensity, and therefore on hairpin end-to-end distance fluctuations).

Time intervals where acceptor counts were lower to or equal to the threshold value ($2 \times (\langle B_A \rangle + \langle C_A \rangle)^{(1/2)}$) were removed from the intensity time trajectories (see also Fig. S2 in Supplementary Material).

Single molecule cross correlation of $I_D(t)$ versus $I_A(t)$ were calculated with Eq. 5.

$$C(\tau) = \frac{\langle \delta I_D(t) \times \delta I_A(t+\tau) \rangle}{\langle I_D \rangle \times \langle I_A \rangle} = \frac{\langle I_D(t) \times I_A(t+\tau) \rangle}{\langle I_D \rangle \times \langle I_A \rangle} - 1 \quad (5)$$

Each single molecule cross correlation curve was normalized to E_{app} autocorrelation under the assumption that $I_A(t) + I_D(t) =$ constant, that is: $\delta I_A(t) = -\delta I_D(t)$

Under this assumption the E_{app} autocorrelation equals the I_A autocorrelation (Eq.6).

$$E_{app}Autocorrelation(\tau) = \frac{\langle \delta E_{app}(t) \times \delta E_{app}(t+\tau) \rangle}{\langle E_{app} \rangle \times \langle E_{app} \rangle} = \frac{\langle \delta I_A(t) \times \delta I_A(t+\tau) \rangle}{\langle I_A \rangle \times \langle I_A \rangle} \quad (6)$$

Replacing $\delta I_D(t)$ by $-\delta I_A(t)$ in Eq. 5 we get:

$$C(\tau) = \frac{\langle -\delta I_A(t) \times \delta I_A(t+\tau) \rangle}{\langle I_D \rangle \times \langle I_A \rangle} \quad (7)$$

Multiplying Eq. 7 by $(-\langle I_D \rangle / \langle I_A \rangle)$ the cross correlation is normalized to the E_{app} autocorrelation; see Eq. 8:

$$E_{app}Autocorrelation(\tau) = C(\tau) \times \left(-\frac{\langle I_D \rangle}{\langle I_A \rangle} \right) \quad (8)$$

We averaged the single molecule E_{app} autocorrelation curves obtained under a set of experimental conditions (with or without NC).

Donor-acceptor cross correlations were also obtained with an ALV 5000/E correlation board with 0.5-μs time resolution. Data were acquired for a total of 4 s. The data from any single molecule that photobleached before finishing acquisition were discarded.

RESULTS AND DISCUSSION

HIV-1 NC effect on the distribution of hairpin end-to-end distances

We recorded the trajectory and the distribution of $E_{app}(t)$ for single molecules of various donor-acceptor (Cy3-Cy5) labeled DNA hairpin constructs with different numbers of internal bulges (see Fig. 1). We determined the number of hairpin stems affected by NC by comparing the data acquired with the different constructs in the presence and absence of NC. Previous work has demonstrated that maximum NC destabilizing activity is obtained under saturating protein concentrations, where one NC protein is bound to eight nucleotides (Rein et al., 1998; Williams et al., 2001). Maximum annealing rates between TAR DNA and TAR RNA hairpins occur for $[NC] \geq 500$ nM (Guo et al., 2002). Our experiments were performed with saturating NC concentrations close to this range.

Any single molecule is representative of the ensemble under our experimental conditions, i.e., the system is ergodic. Individual single molecule trajectories and distributions of $E_{app}(t)$ are indistinguishable from each other when recorded under the same experimental conditions. The mean E_{app} values measured for individual single molecules ($\langle E_{app} \rangle_{mol}$) are also very similar to each other (Fig. 2, *left column*; see also Fig. S3 in Supplementary Material).

Hairpins with two or more internal bulges are predominantly found with the two terminal stems open at equilibrium with 445 nM NC. An $\langle E_{app} \rangle_{mol} \sim 0.77$, $\sigma_{Eapp} = 0.07$ was measured for TAR DNA single molecules with NC

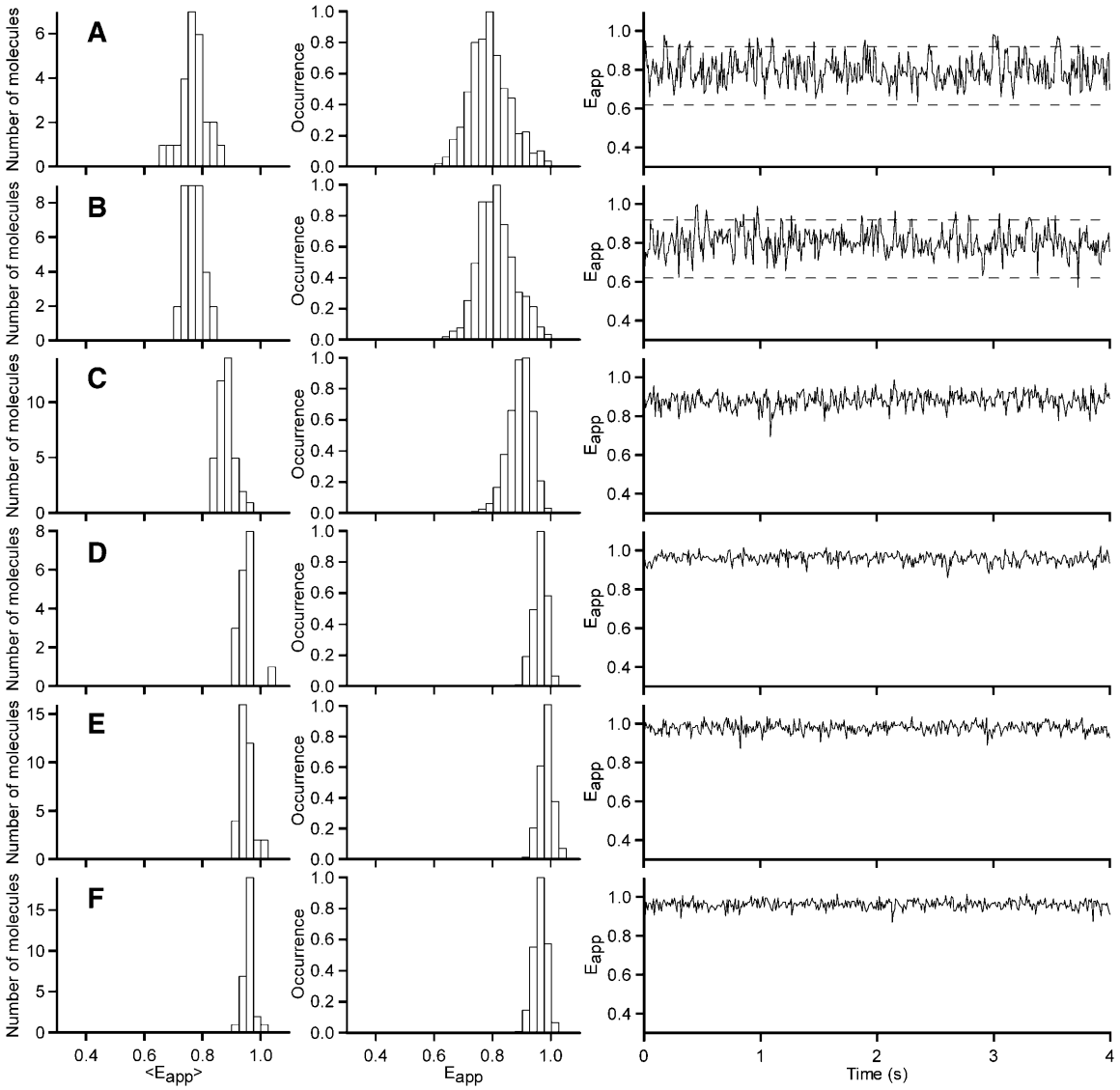

FIGURE 2 (*Left column*) Distribution of $\langle E_{app}\rangle_{mol}$ values. (*Middle and right columns*) Distribution and trajectory of $E_{app}(t)$ for a representative single molecule (10-ms binning). Panels *A–D* correspond to data acquired with 445 nM NC and 0.2 mM $MgCl_2$. (*A*) TAR DNA single molecules. (*B*) -L4-L3 mutant single molecules. (*C*) -L4-L3-L2 mutant single molecules. (*D*) -L4-L3-L2-L1 mutant single molecules. Also shown are the corresponding figures for (*E*) -L4-L3 mutant and (*F*) -L4-L3-L2-L1 mutant in the absence of NC and with 0.2 mM $MgCl_2$. Overlaid on the trajectories of TAR DNA/NC and -L4-L3 mutant/NC (*A* and *B*) is shown the 99% confidence interval for a distribution centered at $E_{app} = 0.77$. Any point outside the range ($\pm$ 2.6 $\times$ $\sigma_{Eapp=0.77}$) does not correspond to an open conformation, where $\sigma_{Eapp=0.77}$ is the standard deviation estimated from shot noise for $E_{app} = 0.77$ (see Fig. S4 and the discussion therein in the Supplementary Material).

flowed at a rate of 2 μl/min (Fig. 2 *A*). The same values were obtained for mutant forms of TAR DNA hairpins for which the internal bulge L4 (see Fig. 1 *B*) and both internal bulges L4 and L3 (see Fig. 1 *C*) were deleted (see Fig. 2 *B*). Inspection of the single molecule trajectories of $E_{app}(t)$ reveals that the hairpins sporadically closed to the conformation with $E_{app} \sim 1$ (see *right columns* in Fig. 2, *A* and *B*). The closing events are also evident from the unsymmetrical distribution of $E_{app}(t)$ (see Fig. 2, *A* and *B*). From the distribution of $E_{app}(t)$, as much as 10% of the events can be assigned to a closed hairpin conformation.

NC induces larger donor-acceptor dye separations in a structure with two internal bulges compared to one internal bulge. Thus the distribution of $E_{app}(t)$ for a third TAR DNA mutant form conserving only the terminal internal loop (-L4-L3-L2, Fig. 1 *D*) has a mean value $\langle E_{app}\rangle_{mol} = 0.90$, $\sigma_{Eapp} = 0.05$ with 445 nM NC (see Fig. 2 *C*).

A TAR DNA mutant for which all four internal loops were deleted (-L4-L3-L2-L1, Fig. 1 *E*) is characterized by a fully closed conformation with or without NC, $\langle E_{app}\rangle_{mol} \sim 0.97$, $\sigma_{Eapp} = 0.04$ (Fig. 2, *D* and *F*, respectively). In fact, the individual $E_{app}(t)$ trajectories for this TAR DNA mutant with

or without NC are indistinguishable from trajectories for -L4-L3 mutant hairpins without NC (Fig. 2 *E*). This result confirms previous reports on the critical importance of internal bulges in the hairpin structure to observe an NC effect (Beltz et al., 2003).

The data provide direct evidence at the individual hairpin level that NC activity in TAR DNA is limited to internal loops L1 and L2 and does not involve the internal bulges L3 and L4 (see Scheme 1). Thus, all hairpin constructs conserving the two internal loops L1 and L2 have identical distributions of $E_{app}(t)$ when complexed with NC, irrespective of the presence of other destabilizing internal bulges. In comparison, the hairpin conserving only the last internal loop can only access a conformation with a smaller end-to-end distance when complexed with NC. Finally, the construct where all the internal loops and bulges have been deleted is only found in the closed conformation.

Approximately 20% of the single molecules observed for TAR DNA/NC (but not any of the mutant hairpin structures) exhibited extremely slow FRET dynamics (relaxation lifetimes $\gg$1 s) with slowly varying E_{app} amplitude changes. We assign the single molecules with slow dynamics to hairpins that are perturbed by binding to the BSA surface. This is supported by the following observations: 1), analogous slow FRET dynamics are not observed in bulk ensemble FRET measurements on nonimmobilized TAR/DNA; 2), a slight increase of the $MgCl_2$ concentration in the buffer suppresses the formation of slow FRET hairpins, due presumably to better hairpin/surface screening; and 3), FRET dynamics on the many-second timescale is too slow to be associated with DNA hairpin opening/closing reactions.

Care has been taken to rule out any influence that fluorophore blinking (reversible photobleaching) or fluorophore quenching by NC might have on the observed trajectories and distributions of $E_{app}(t)$. Thus, we note that no emission quenching is observed upon NC addition to the construct that lacks internal loops and bulges. On the other hand, Cy5 blinking events were removed from the $E_{app}(t)$ trajectories as described in the Experimental Setup section. We conclude that the $\langle E_{app}\rangle_{mol} < 0.97$ observed in hairpins with internal loops/bulges (Fig. 2, *A–C*) in equilibrium with NC is a direct result of NC-hairpin interactions.

Consistent with a closed hairpin structure, the distribution of $E_{app}(t)$ values for -L4-L3 mutant single molecules in the absence of NC has a mean value $\langle E_{app}\rangle_{mol} = 0.97$, $\sigma_{Eapp} = 0.04$, (Fig. 2 *E*). Fig. 3 portrays the normalized ensemble distributions of $E_{app}(t)$ for the different hairpins with and without NC to facilitate their comparison.

HIV-1 NC effect on dynamics of hairpin end-to-end distances

Hairpin opening-closing relaxation rate constants k_r were obtained from cross correlation analyses of the single molecule donor-acceptor intensity time trajectories. Briefly, in this analysis fluorescence intensity fluctuations in the donor channel are correlated with fluorescence intensity fluctuations in the acceptor channel to quantify the temporal evolution of the system in equilibrium (Hess et al., 2002). From the cross-correlation analyses we were able to assign the rate constants associated with the observed hairpin conformational distributions.

The correlation analysis of the data reveals dynamics in the milliseconds time domain for hairpins with one or more internal bulges in equilibrium with NC. Consistent with dynamics reflecting FRET efficiency fluctuations, donor and

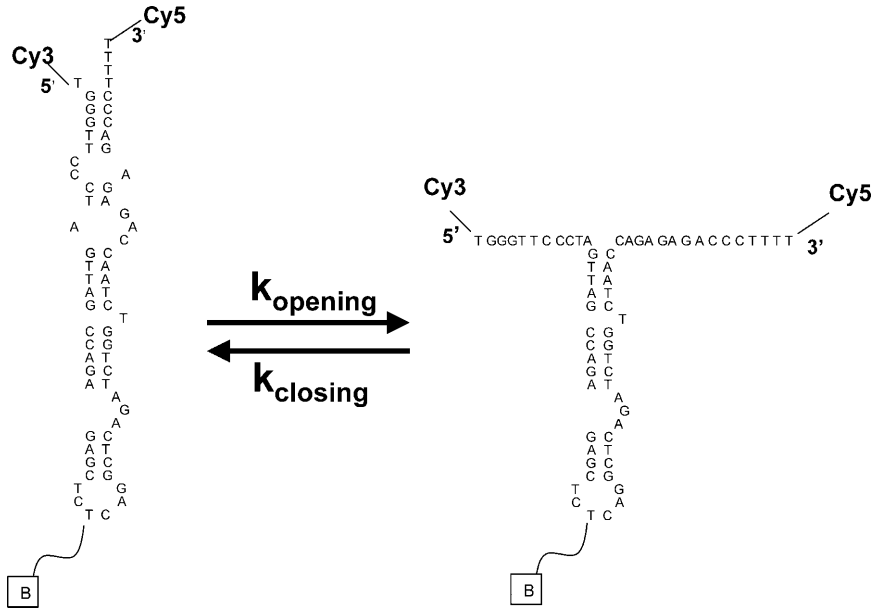

SCHEME 1 Hairpin dynamics with 445 nM NC.

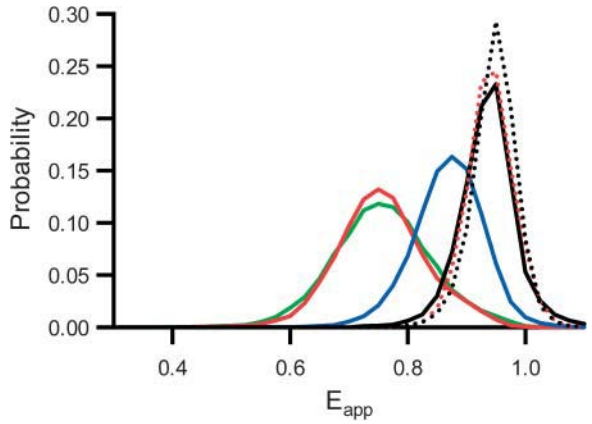

FIGURE 3 Normalized ensemble distribution of $E_{app}(t)$ (constructed by combining the individual single molecule distribution of $E_{app}(t)$ acquired with 10-ms time resolution). Curves correspond to TAR DNA (*green*), -L4-L3 mutant (*red*), -L4-L3-L2 mutant (*blue*), and -L4-L3-L2-L1 mutant (*black*). All measurements were carried out in the presence of 445 nM NC and 0.2 mM $MgCl_2$. Also shown are the normalized ensemble distribution of $E_{app}(t)$ for -L4-L3 mutant (*dashed red line*) and -L4-L3-L2-L1 mutant (*dashed black line*) in the absence of NC and with 0.2 mM $MgCl_2$.

acceptor intensities are anticorrelated; i.e., an increase in donor intensity is accompanied by a decrease in acceptor intensity (Kim et al., 2002). Cross correlations were converted to E_{app} autocorrelations as described in the Experimental Setup section.

Table 1 lists the relaxation rate constants and amplitudes derived from the cross-correlation analysis of $I_A(t)$ and $I_D(t)$ trajectories for TAR DNA/NC, -L4-L3 mutant/NC, and -L4-L3-L2 mutant/NC (see columns 1 and 2). A single exponential relaxation with a rate constant $k_r = 4 \times 10^2\ s^{-1}$ was measured for -L4-L3-L2 mutant/NC. The single exponential decay indicates that this is a two-state transition between an open and a closed hairpin conformation. The E_{app} autocorrelation relaxation rate constants for TAR DNA/NC and for -L4-L3 mutant/NC have values of $k_r = 3 \times 10^2\ s^{-1}$ and $2 \times 10^2\ s^{-1}$, respectively. Conformational equilibration (relaxation) occurs on a timescale of a few milliseconds, much shorter than the observation time (~4–20 s) for each hairpin, ensuring equilibrium sampling in the observed single molecule data.

The relaxation rate constant in a two-state system (open-closed) depends linearly on both opening and closing rate constants ($k_r = k_{opening} + k_{closing}$) (Cantor and Schimmel, 1980). The predominantly open hairpin conformation directly observed from the distribution of $E_{app}(t)$ reveals that for TAR DNA/NC or -L4-L3 mutant/NC the opening rate constant is much larger than the closing rate constant. As much as 10% of the E_{app} events can be assigned to a closed hairpin conformation. In a two-state model this would indicate that opening and closing rate constants for TAR DNA/NC or -L4-L3/NC are in the range between $k_{closing} \leq 3 \times 10^1\ s^{-1}$ and $k_{opening} \geq 2.5 \times 10^2\ s^{-1}$.

In an attempt to shift the equilibrium from the predominantly open hairpin conformation directly observed from the distribution of $E_{app}(t)$ for TAR DNA/NC and -L4-L3 mutant/NC we increased the $MgCl_2$ concentration by ~10-fold. Fig. 4 illustrates the distribution of $\langle E_{app} \rangle_{mol}$ values (*left*) and a representative single molecule $E_{app}(t)$ distribution (*middle*) and time trajectory (*right*) in the presence of 2.5 mM $MgCl_2$. Consistent with a stabilization of the closed hairpin by $MgCl_2$ (Misra and Draper, 1998) the equilibrium was shifted to the closed conformation after addition of 2.5 mM $MgCl_2$. Under these conditions the measured relaxation rate constant is $\sim 0.7 \times 10^2\ s^{-1}$ and the closed-open equilibrium constant is $K_{closed\text{-}open} \sim 1$. If a two-state model applies to these conditions opening and closing rate constants for -L4-L3 mutant/NC are $k_{closing} \sim k_{opening} = 0.4 \times 10^2\ s^{-1}$. Two distinct peaks at ~0.8 and 0.97 were resolved in the distribution of $E_{app}(t)$. These observations support the conclusion that the dynamics of hairpin opening-closing relaxation in the presence of NC occur in the millisecond time domain.

The observation of large amplitude NC-induced DNA conformational fluctuations on the millisecond timescale

TABLE 1 E_{app} autocorrelation relaxation rate constants and amplitudes for various hairpins in the presence of 445 nM NC and with no NC

Hairpin construct	*k_r (s^{-1})	*A	†k_r1 (s^{-1})	†A_1	†k_r2 (s^{-1})	†A_2
TAR DNA/NC	3×10^2	6×10^{-3}	2×10^2	8×10^{-3}	3×10^3	10×10^{-3}
-L4-L3/NC	2×10^2	6×10^{-3}	2×10^2	8×10^{-3}	2×10^3	9×10^{-3}
‡-L4-L3/NC	0.7×10^2	2×10^{-3}	0.8×10^2	4×10^{-3}	0.6×10^3	3×10^{-3}
-L4-L3-L2/NC	4×10^2	2×10^{-3}	5×10^2	6×10^{-3}	–	–
-L4-L3-L2-L1/NC	§N.A.	§0	§N.A.	§0	–	–
-L4-L3	§N.A.	§0	§N.A.	§0	–	–
-L4-L3-L2-L1	§N.A.	§0	§N.A.	§0	–	–

*Obtained from the analysis of $I_A(t)$ and $I_D(t)$ trajectories (from 1 ms to 4 s).

†Simultaneously measured with an ALV 5000/E correlation board (from 0.5 μs to 4 s).

‡Measured in the presence of 2.5 mM $MgCl_2$. Cross correlations were converted to E_{app} autocorrelation as described in the Experimental Setup section. The correlations of individual single molecules were averaged to obtain the reported ensemble value. The error in the reported values (±50%) was determined from the standard deviation of the distributions of k_r and A for individual single molecules.

§N.A. indicates not assigned. Amplitudes $\leq 0.5 \times 10^{-3}$ are indistinguishable from noise; therefore the relaxation rate constant values could not be assigned.

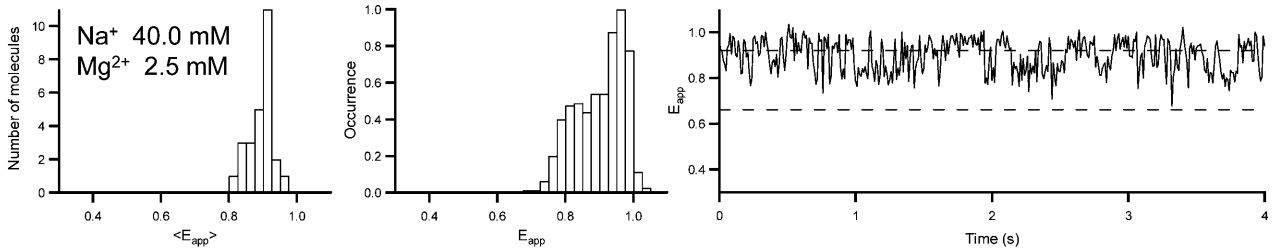

FIGURE 4 (*Left panel*) Distribution of $\langle E_{app}\rangle_{mol}$ values. (*Middle and right panels*) Distribution and trajectory of $E_{app}(t)$ for a representative single molecule (10-ms binning). Data acquired with -L4-L3 mutant/NC with 445 nM NC and 2.5 mM $MgCl_2$.

reported here is in contrast to previous work reporting NC-induced DNA conformational fluctuations on the microsecond timescale (Azoulay et al., 2003; Beltz et al., 2003). The latter study was carried out using fluorescence correlation spectroscopy (FCS), a technique that is unable to measure slow dynamics, using a related cTAR DNA and truncated NC system.

To determine if faster events escaped our detection, we cross correlated the donor and acceptor intensities of single immobilized hairpins over a time range from 0.5 μs to 4 s with an ALV5000/E correlator board. Fig. 5 portrays the ensemble E_{app} autocorrelation derived from donor-acceptor cross correlations. No fast components are observed in -L4-L3-L2 mutant/NC for which the relaxation rate is similar to that obtained from the $E_{app}(t)$ trajectories (Table 1; compare columns 2 and 4). The relaxation for TAR DNA/NC and -L4-L3 mutant/NC spanned from microseconds to milliseconds with approximately equal weights in both time domains. A biexponential fit to the data generates relaxation rate constants of $2 \times 10^2\ s^{-1}$ and $3 \times 10^3\ s^{-1}$ for TAR DNA/NC and $2 \times 10^2\ s^{-1}$ and $2 \times 10^3\ s^{-1}$ for -L4-L3 mutant/NC, respectively (Table 1; columns 4 and 6). In the presence of 2.5 mM $MgCl_2$, the decay for -L4-L3 mutant/NC is bi-exponential with relaxation rate constants of $0.8 \times 10^2\ s^{-1}$ and $6 \times 10^2\ s^{-1}$.

Although we have not been able to assign the TAR DNA hairpin conformational distribution associated with the fast relaxation dynamics observed in the correlation analysis ($k_r = 3 \times 10^3\ s^{-1}$), it is not surprising that such a complex system involving the interaction of many NC proteins with the TAR DNA hairpin exhibits multiexponential opening-closing relaxations.

We performed control experiments to determine the effect, if any, that Cy5 photophysical properties have on the correlation curves measured (Widengren et al., 2001; Widengren and Schwille, 2000). Experiments were done with the -L4-L3 mutant in the absence of NC and with the -L4-L3-L2-L1 mutant in the absence and presence of NC. The cross correlation for the controls had an amplitude $\sim$0 after 2×10^{-4} s. There were no donor-acceptor anticorrelated fluctuations with lifetimes of 100 μs or longer. Cross correlations at times $< 2 \times 10^{-4}$ s appear to be dominated by Cy5 *cis-trans* isomerization, unrelated to FRET dynamics. A more complete discussion of the early time behavior of the autocorrelation is given in the Supplementary Material.

There is no measurable change in the single molecule data when BSA is replaced by an alternative surface coating, polyethyleneglycol (PEG). This strongly suggests that surface interactions are not significant because these surfaces are known to present very different chemical environments. The $E_{app}(t)$ distribution mean value and standard deviation and the E_{app} autocorrelation amplitudes and relaxation rate constants are the same within experimental error for PEG and BSA. In particular, results on the effect of NC complexation on the TAR DNA hairpin end-to-end dynamics and end-to-end equilibrium distribution obtained with polyethylenegly-

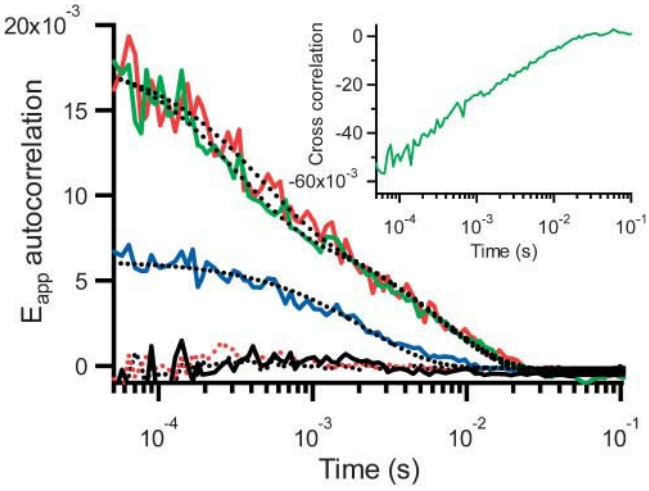

FIGURE 5 Ensemble E_{app} autocorrelation and fit to the experimental data. Each ensemble was constructed by combining the single molecule E_{app} autocorrelations of individual immobilized hairpins of TAR DNA (*green*), -L4-L3 mutant (*red*), -L4-L3-L2 mutant (*blue*), and -L4-L3-L2-L1 mutant (*black*) in the presence of 445 nM NC and 0.2 mM $MgCl_2$. The inset shows the corresponding ensemble cross correlation for TAR DNA. A minimum of 18 single molecules were analyzed in each case. Also shown are the ensemble E_{app} autocorrelation for the -L4-L3 mutant (*dashed red line*) and -L4-L3-L2-L1 mutant (*dashed black line*) in the absence of NC and with 0.2 mM $MgCl_2$. The autocorrelation curves at times $< 5 \times 10^{-5}$ s have been omitted from this figure because they are dominated by Cy5 photophysical events that are unrelated to the FRET behavior. A more complete discussion of the early time behavior of the autocorrelation is given in the Supplementary Material (see Figs. S5 and S6).

col (MW 2000, Nektar Therapeutics, Huntsville, AL) and biotinylated polyethyleneglycol (MW 5000, Nektar Therapeutics) coated coverslips (see Fig. S7 in Supplementary Material) (Ha, 2001; Rasnik et al., 2004) are identical to those obtained with the BSA-based immobilization scheme reported here.

CONCLUSIONS

To elucidate the secondary structure of potential intermediates in the NC-catalyzed annealing process, we have undertaken the first time-resolved SM-FRET measurements on TAR DNA hairpins and hairpin mutants complexed with NC. The data were analyzed to determine the effect of NC complexation on the DNA end-to-end dynamics and end-to-end equilibrium distribution. The data show that NC shifts the equilibrium secondary structure of TAR DNA hairpins from a fully ''closed'' conformation to a ''partially open'' conformation with the two terminal stems ''open'' or unwound and the other stems closed. Conformational equilibration (relaxation) occurs on a timescale (~1 ms) much shorter than the observation time (~4–20 s) for each hairpin insuring equilibrium sampling in the observed single molecule data. It can be argued that the observed partially open TAR DNA/NC conformation is a critical intermediate in the NC catalyzed annealing mechanism of TAR DNA/RNA, because the open terminal stems possess 21 unpaired bases that are accessible for DNA/RNA annealing.

SUPPLEMENTARY MATERIAL

An online supplement to this article can be found by visiting BJ Online at http://www.biophysj.org.

We thank Dr. Nick Lee and Mr. Minh Hong for purification of NC protein and Dr. Ioulia Rouzina for helpful discussions.

This research was supported by National Institutes of Health (NIH) grant AI43231 (K.M.F.), NIH grant GM65818 (P.F.B.), and NIH postdoctoral National Research Service Award grant F32 AI10463 (E.J.H.).

REFERENCES

Azoulay, J., J.-P. Clamme, J.-L. Darlix, B. P. Roques, and Y. Mély. 2003. Destabilization of the HIV-1 complementary sequence of TAR by the nucleocapsid protein through activation of conformational fluctuations. *J. Mol. Biol.* 326:691–700.

Beltz, H., J. Azoulay, S. Bernacchi, J.-P. Clamme, D. Ficheux, B. Roques, J.-L. Darlix, and Y. Mély. 2003. Impact of the terminal bulges of HIV-1 cTAR DNA on its stability and the destabilizing activity of the nucleocapsid protein NCp7. *J. Mol. Biol.* 328:95–108.

Bernacchi, S., S. Stoylov, E. Piemont, D. Ficheux, B. P. Roques, J. L. Darlix, and Y. Mély. 2002. HIV-1 Nucleocapsid protein activates transient melting of least stable parts of the secondary structure of TAR and its complementary sequence. *J. Mol. Biol.* 317:385–399.

Cantor, C. R., and P. R. Schimmel. 1980. Part III: The Behavior of Biological Macromolecules. C. R. Cantor and P. R. Schimmel, editors. W. H. Freeman and Company, San Francisco, CA.

Coffin, J. M., S. H. Hughes, and H. E. Varmus. 1997. Retroviruses. Cold Spring Harbor Laboratory Press, Cold Spring Harbor, NY.

Darlix, J.-L., M. Lapadat-Tapolsky, H. de Rocquigny, and B. P. Roques. 1995. First glimpses at structure-function relationships of the nucleocapsid protein of retroviruses. *J. Biol. Chem.* 254:523–537.

Driscoll, M. D., and S. H. Hughes. 2000. Human immunodeficiency virus type 1 nucleocapsid protein can prevent self-priming of minus-strand strong stop DNA by promoting the annealing of short oligonucleotides to hairpin sequences. *J. Virol.* 74:8785–8792.

English, D. S., A. Furube, and P. F. Barbara. 2000. Single molecule spectroscopy in oxygen depleted polymer films. *Chem. Phys. Lett.* 324:15–19.

Grunwell, J. R., J. L. Glass, T. D. Lacoste, A. A. Deniz, D. S. Chemla, and P. G. Schultz. 2001. Monitoring the conformational fluctuations of DNA hairpins using single-pair fluorescence resonance energy transfer. *J. Am. Chem. Soc.* 123:4295–4303.

Guo, J., L. E. Henderson, J. Bess, B. Kane, and J. G. Levin. 1997. Human immunodeficiency virus type 1 nucleocapsid protein promotes efficient strand transfer and specific viral DNA synthesis by inhibiting TAR-dependent self-priming from minus-strand strong-stop DNA. *J. Virol.* 71:5178–5188.

Guo, J., T. Wu, B. F. Kane, D. J. Johnson, L. E. Henderson, R. J. Gorelick, and J. G. Levin. 2002. Subtle alterations of the native zinc finger structures have dramatic effects on the nucleic acid chaperone activity of human immunodeficiency virus type 1 nucleocapsid protein. *J. Virol.* 76:4370–4378.

Ha, T. 2001. Single-molecule fluorescence resonance energy transfer. *Methods.* 25:78–86.

Ha, T., I. Rasnik, W. Cheng, H. P. Babcock, G. Gauss, T. M. Lohman, and S. Chu. 2002. Initiation and reinitiation of DNA unwinding by the Escherichia coli Rep helicase. *Nature.* 419:638–641.

Ha, T., X. W. Zhuang, H. D. Kim, J. W. Orr, J. R. Williamson, and S. Chu. 1999. Ligand-induced conformational changes observed in single RNA molecules. *Proc. Natl. Acad. Sci. USA.* 96:9077–9082.

Harada, Y., K. Sakurada, T. Aoki, D. D. Thomas, and T. Yanagida. 1990. Mechanochemical coupling in actomyosin energy transduction studied by in vitro movement assay. *J. Mol. Biol.* 216:49–68.

Henderson, L. E., M. A. Bowers, R. C. I. Sowder, S. A. Serabyn, D. G. Johnson, J. W. J. Bess, L. O. Arthur, D. K. Bryant, and C. Fenselau. 1992. Gag proteins of the highly replicative MN strain of human immunodeficiency virus type 1: posttranslational modifications, proteolytic processings, and complete amino acid sequences. *J. Virol.* 66:1856–1865.

Herchslag, D. 1995. RNA chaperones and the RNA folding problem. *J. Biol. Chem.* 270:20871–20874.

Hess, S. T., S. Huang, A. A. Heikal, and W. W. Webb. 2002. Biological and chemical applications of fluorescence correlation spectroscopy: a review. *Biochemistry.* 41:697–705.

Hong, M. K., E. J. Harbron, D. B. O'Connor, J. Guo, P. F. Barbara, J. G. Levin, and K. Musier-Forsyth. 2003. Nucleic acid conformational changes essential for HIV-1 nucleocapsid protein-mediated inhibition of self-priming in minus-strand transfer. *J. Mol. Biol.* 325:1–10.

Kim, H. D., G. U. Nienhaus, T. Ha, J. W. Orr, J. R. Williamson, and S. Chu. 2002. Mg2+-dependent conformational change of RNA studied by fluorescence correlation and FRET on immobilized single molecules. *Proc. Natl. Acad. Sci. USA.* 99:4284–4289.

Kim, J. K., C. Palaniappan, W. Wu, P. J. Fay, and R. A. Bambara. 1997. Evidence for a unique mechanism of strand transfer from the transactivation response region of HIV-1. *J. Biol. Chem.* 272:16769–16777.

Kurata, S., T. Kanagawa, K. Yamada, M. Torimura, T. Yokomaku, Y. Kamagata, and R. Kurane. 2001. Fluorescent quenching-based quantitative detection of specific DNA/RNA using a BODIPY((R)) FL-labeled probe or primer. *Nucleic Acids Res.* 29:E34.

Lakowicz, J. R. 1999. Energy Transfer. Principles of Fluorescence Spectroscopy. Kluwer Academic, New York, NY.

Lapadat-Tapolsky, M., C. Gabus, M. Rau, and J.-L. Darlix. 1997. Possible roles of HIV-1 nucleocapsid protein in the specificity of proviral DNA synthesis and in its variability. *J. Mol. Biol.* 268:250–260.

Lee, B. M., R. N. De Guzman, B. G. Turner, N. Tjandra, and M. F. Summers. 1998. Dynamical behavior of the HIV-1 nucleocapsid protein. *J. Mol. Biol.* 279:633–649.

Lorsch, J. R. 2002. RNA chaperones exist and DEAD box proteins get a life. *Cell.* 109:797–800.

Misra, V. K., and D. E. Draper. 1998. On the role of magnesium ions in RNA stability. *Biopolymers.* 48:113–135.

Rasnik, I., S. Myong, W. Cheng, T. M. Lohman, and T. Ha. 2004. DNA-binding orientation and domain conformation of the E. coli Rep helicase monomer bound to a partial duplex junction: single-molecule studies of fluorescently labeled enzymes. *J. Mol. Biol.* 336:395–408.

Rein, A., L. E. Henderson, and J. G. Levin. 1998. Nucleic-acid-chaperone activity of retroviral nucleocapsid proteins: significance for viral replication. *Trends Biochem. Sci.* 23:297–301.

South, T. L., B. Kim, D. R. Hare, and M. F. Summers. 1990. Zinc fingers and molecular recognition. structure and nucleic acid binding studies of an HIV zinc finger-like domain. *Biochem. Pharmacol.* 40:123–129.

Summers, M. F., L. E. Henderson, M. R. Chance, J. W. Bess, Jr., T. L. South, P. R. Blake, I. Sagi, G. Perez-Alvarado, R. C. Sowder III, D. R. Hare, et al. 1992. Nucleocapsid zinc fingers detected in retroviruses: EXAFS studies of intact viruses and the solution-state structures of the nucleocapsid protein from HIV-1. *Protein Sci.* 1:563–574.

Torimura, M., S. Kurata, K. Yamada, T. Yokomaku, Y. Kamagata, T. Kanagawa, and R. Kurane. 2001. Fluorescence-quenching phenomenon by photoinduced electron transfer between a fluorescent dye and a nucleotide base. *Anal. Sci.* 17:155–160.

Tsuchihashi, Z., and P. O. Brown. 1994. DNA strand exchange and selective DNA annealing promoted by the human immunodeficiency virus type 1 nucleocapsid protein. *J. Virol.* 68:5863–5870.

Widengren, J., E. Schweinberger, S. Berger, and C. A. M. Seidel. 2001. Two new concepts to measure fluorescence resonance energy transfer via fluorescence correlation spectroscopy: theory and experimental realizations. *J. Phys. Chem. A.* 105:6851–6866.

Widengren, J., and P. Schwille. 2000. Characterization of photoinduced isomerization and back-isomerization of the cyanine dye Cy5 by fluorescence correlation spectroscopy. *J. Phys. Chem. A.* 104:6416–6428.

Williams, M. C., I. Rouzina, J. R. Wenner, R. J. Gorelick, K. Musier-Forsyth, and V. A. Bloomfield. 2001. Mechanism for nucleic acid chaperone activity of HIV-1 nucleocapsid protein revealed by single molecule stretching. *Proc. Natl. Acad. Sci. USA.* 98:6121–6126.

Ying, L., M. I. Wallace, S. Balasubramanian, and D. Klenerman. 2000. Ratiometric analysis of single-molecule fluorescence resonance energy transfer using logical combinations of threshold criteria: a study of 12-mer DNA. *J. Phys. Chem. B.* 104:5171–5178.

Yip, W.-T., D. Hu, J. Yu, D. A. Vanden Bout, and P. F. Barbara. 1998. Classifying the photophysical dynamics of single- and multiple-chromophoric molecules by single molecule spectroscopy. *J. Phys. Chem. A.* 102:7564–7575.

You, J. C., and C. S. McHenry. 1994. Human immunodeficiency virus nucleocapsid protein accelerates strand transfer of the terminally redundant sequences involved in reverse transcription. *J. Biol. Chem.* 269:31491–31495.

Zhuang, X. W., L. E. Bartley, H. P. Babcock, R. Russell, T. J. Ha, D. Herschlag, and S. Chu. 2000. A single-molecule study of RNA catalysis and folding. *Science.* 288:2048–2051.